Bis(9-Boraphenanthrene) and its Stable Biradical

Samir Kumar Sarkar,[1] Kimberly K. Hollister,[1] Andrew Molino,[2] Akachukwu D. Obi,[2] Chun-Lin Deng,[1] Bi Youan E. Tra,[1] Brennan M. Stewart,[3] Diane A. Dickie,[3] David J. D. Wilson,*[2] and Robert J. Gilliard, Jr*[1]

[1]Department of Chemistry, Massachusetts Institute of Technology, Cambridge, Massachusetts 02139, United States

[2]Department of Biochemistry and Chemistry, La Trobe Institute for Molecular Science, La Trobe University, Melbourne 3086 Victoria, Australia

[3]Department of Chemistry, University of Virginia, Charlottesville, Virginia 22904, United States

Supporting Information Placeholder

ABSTRACT: Selective and site-specific boron-doping of polycyclic aromatic hydrocarbon frameworks often give rise to redox and/or photophysical properties that are not easily accessible with the analogous all-carbon systems. Herein, we report ligand-mediated control of boraphenanthrene closed- and open-shell electronic states, which has led to the first structurally characterized examples of neutral bis(9-boraphenanthrene) (**2**-**3**) and its corresponding biradical (**4**). Notably, compounds **2** and **3** show intramolecular charge transfer absorption from the 9-boraphenanthrene units to *p*-quinodimethane, exhibiting dual (red-shifted) emission in solution due to excited state conjugation enhancement (ESCE). Moreover, while boron-centered monoradicals are ubiquitous, biradical **4** represents a rare type of open-shell singlet compound with 95% biradical character, among the highest of any reported boron-based polycyclic species with two radical sites.

■ INTRODUCTION

Since its discovery by Fittig and Ostermayer 150 years ago,[1a,b] phenanthrene (Figure 1a), a tricyclic system consisting of three fused benzene rings, has found numerous applications as components of organic dyes, drugs, and pesticides.[1-3] However, it is most often used as a key building block for the synthetic elaboration of conjugated materials.[3b-d] While the chemistry of all-carbon phenanthrene has been thoroughly investigated, "inorganic" boron-doped analogues are extremely rare. Molecules that incorporate boron in specific positions of π-electron systems are highly sought-after and have led to new types of organic light emitting diodes (OLEDs), semiconductors, solar cells, organic field-effect transistors, nanoscale electronic devices, as well as in nonlinear optics (NLO).[4-9] They have also served as a means to explore fundamental chemistry concepts including aromaticity, chemical bonding, and periodic trends.[10] The distinct electronic and photophysical properties of boracycles are a direct result of boron's electron-deficient nature, possessing an empty p_z orbital which permits facile electronic structure modification and redox chemistry. Despite the beneficial characteristics of these compounds, they can be challenging to experimentally isolate and characterize. To date, only one boraphenanthrene has been reported−the 9-borataphenanthrene anion (Figure 1b).[11] Neutral 9-boraphenanthrene and 9-boraphenanthrene radicals are hitherto unknown (Figure 1c and d). Recently, we described the synthesis of a cyclic(alkyl)(amino) carbene (CAAC)-stabilized BP-doped phenanthryne, where the boron-adjacent phosphorus atom possesses a lone pair (Figure 1e).[12] This study, coupled with our goal of developing boron systems with unusual luminescent properties, prompted us to target highly conjugated bis(boraphenanthrenes). Furthermore, a carbon-boron (C=B) double bond stabilized by a neutral donor ligand is isosteric and isoelectronic with a C=C bond, and this motif within polycyclic aromatic hydrocarbon (PAH) structures typically lead to a decrease in the HOMO–LUMO energy gaps, permitting access to compounds with red-shifted absorption and emission bands.[13-15]

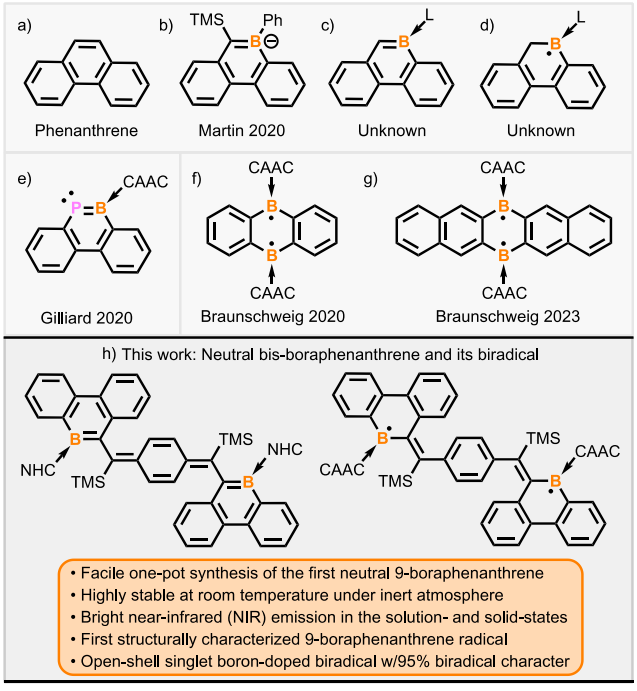

Figure 1. (a) phenanthrene; (b) 9-borataphenanthrene anion; (c) neutral 9-boraphenanthrene; (d) 9-boraphenanthrene radical; (e) BP-phenanthryne; (f) anthracene biradical (g) pentacene biradical; (h) This work: bis(9-boraphenanthrene) and its biradical.

Most of the reported boron-doped PAHs can be characterized by a closed-shell electron configuration.[4-9] In contrast, boron-doped PAHs exhibiting an open-shell singlet configuration are rare

(Figure 1f and g).[16-17] This biradical character emerges only when the biradical resonance structure overcomes the "classical" closed-shell preference due to a combination of strong electronic factors and stabilization energy.[18-20] The stability and reactivity of closed-shell PAHs can be determined by the number of aromatic π-sextet rings they possess (i.e., Clar's aromatic sextet rule).[21-22] Benzenoid PAHs with the same chemical composition with more aromatic sextet rings are more stable and less reactive. In contrast, for open-shell biradical species, the biradical character (γ) increases significantly as more aromatic sextet rings form.[22] However, stabilizing the biradical in its open-shell form is challenging because the formation of two radical centers originates from the inherently unfavorable uncoupling of two paired electrons (i.e., the effective loss of one π-bond). This can be achieved by modulation of design factors that favor the decoupling of electrons (e.g., extended conjugation, gain of aromatic stabilization, loss of antiaromaticity, installing kinetic protection around the radical center to prevent electron delocalization, or ligand-promoted alteration of electronic parameters).[9] Herein, we present a novel synthetic approach which led to the successful isolation of the neutral bis(9-boraphenanthrene) (**2**-**3**) and bis(9-boraphenanthrene) biradical (**4**) (Figure 1g). Notably, compounds **2** and **3** are the first structurally authenticated examples of neutral boraphenanthrenes, and they exhibit near-IR emission which is atypical of carbene-stabilized boracycles. More importantly, **4** represents the first example of an open-shell singlet boron-doped radical with near-pure biradical character (γ = 95%).

■ RESULTS AND DISCUSSION

We began our study by seeking to obtain the neutral, non-reduced bis(chloroboracycle) **1** as a molecular precursor for reduction chemistry. Compound **1** was synthesized by reacting 2 equiv. of 9-chloro-9-borafluorene with 1 equiv. of 1,4-bis((trimethylsilyl)ethynyl)benzene in DCM at room temperature (Scheme 1). After stirring, **1** precipitated out and was collected as an air- and moisture-sensitive yellow solid in 88% yield. In this reaction, the five-membered ring of 9-chloro-9-borafluorene undergoes ring expansion to form the six-membered boraphenanthrene. The reaction proceeds through the formation of a carbocation followed by trimethylsilyl migration to the carbocation center (ESI, Scheme 1.1). The $^{11}B\{^1H\}$ NMR spectrum of **1** (62.3 ppm) is consistent with a tricoordinate boron center while the ^{29}Si NMR resonance appears at -10.9 ppm. The reduction of **1** with potassium graphite (KC_8)[23a] in the presence of 1,3-diisopropylimidazol-2-ylidene (I^iPr),[23b] 1,3,4,5-tetramethylimidazol-2-ylidene (IMe_4),[23b] or (2,6-diisopropylphenyl)-4,4-diethyl-2,2-dimethyl-pyrrolidin-5-ylidene ($^{Et}CAAC$)[23c] in a 1:2:2 molar ratio in THF at room temperature afforded solutions that were different shades of red (Scheme 1). The solutions were filtered, solvent was reduced under vacuum and stored at −37 °C, which resulted in the formation of red block-shaped crystals in 65% (for **2**), 68% (for **3**), and 61% (for **4**) yields. Despite the similarities in the reduction strategies, spectroscopic investigations into **2**-**4** supported distinct ligand-promoted differences in the electronic structures. Combined nuclear magnetic resonance (NMR) spectroscopy and X-ray crystal data analysis (vide infra) for compounds **2** and **3** indicate that a newly formed C=B bond is in conjugation within the 9-boraphenanthrene moiety, resulting in fully aromatic boracyclic cores stabilized by (I^iPr) and (IMe_4), respectively. Indeed, the $^{11}B\{^1H\}$ NMR spectra of compounds **2** and **3** show an upfield-shifted signal at δ = 22.3 and 24.4 ppm, which falls in the aromatic region.[23d] The ^{29}Si NMR resonances for **2** (9.1 ppm) and **3** (8.4 ppm) experience a slight upfield shift compared to **1** (10.9 ppm), indicating that electronic changes propagate to the trimethylsilyl functional group. In notable contrast to **2** and **3**, compound **4** exhibited broad resonances in the ^1H NMR spectrum, suggesting the presence of a species with paramagnetic character. In addition to characterization by multinuclear NMR (^1H, $^{13}C\{^1H\}$, $^{11}B\{^1H\}$, ^{29}Si) and EPR spectroscopy, compounds **1**–**4** were analyzed by elemental analysis, which gave data in the acceptable range for combustion experiments (see SI for details). While **4** is air- and moisture-sensitive, compounds **2** and **3** possess high solid-state air-stability (at room temperature) for a base-stabilized reduced boracycle, showing signs of slow decomposition commencing after 3 days as detected by UV-vis spectroscopy. All compounds are highly stable in the solid-state or in non-halogenated solvents under inert atmosphere for months.

Scheme 1. Synthesis of closed-shell neutral bis(9-boraphenanthrene)s (2-3) and open-shell singlet biradical (4)

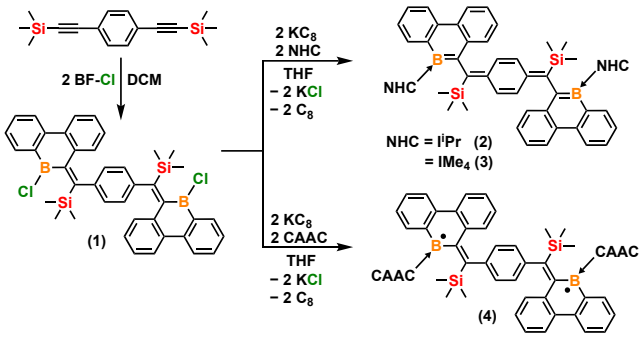

Single crystals of **1**–**4** suitable for X-ray diffraction studies were obtained from a concentrated THF solution at room temperature (Figure 2). In compound **1**, the six-membered boracycles are distorted out-of-plane due to steric hindrance with the −$SiMe_3$ groups [B1−Cl1---H20A−C20 (-$SiMe_3$) distance = 2.73 Å]. Compounds **2** and **3** adopt 'trans' and 'cis' type geometry where both of the boron atoms in 9-boraphenanthrene are opposite each other and stabilized by I^iPr or IMe_4. The 9-boraphenanthrene units are connected by a bis((trimethylsilyl)methylene)cyclohexa-1,4-diene subunit, where the average phenylene C–C (1.45 Å) and C=C (1.34 Å) bond lengths indicate that the quinoidal resonance form has a significant contribution to the ground state electronic structure. The terminal fused benzene rings which are attached to the borabenzene fragment of the 9-boraphenanthrene units slightly deviate from planarity (5.50° and 7.30° for **2** and **3** respectively), caused by steric congestion at the boron center. The $^{carbene}C$−B bond distances are similar in both the molecules [B1−C41: 1.604(3), B2−C52: 1.609(3) Å for **2** and B1−C7: 1.604(3), B2−C48: 1.594(4) Å for **3**]. The newly formed endocyclic B=C double bonds are equal within standard deviation [B1-C13: 1.469(4) Å, B2-C22: 1.473(3) for **2**; B1-C20: 1.467(4) Å, B2-C35: 1.475(4) Å for **3**)] and shorter than the reported B=C bond (1.497 Å) in the 9-borataphenanthrene anion.[15] Crystallographic analysis of **4** reveal trigonal planar geometry around the boron centers. The B1–C13 bond [1.619(4) Å] is significantly longer than the B1–C13 bond [1.545(4) Å] in **1** due to the steric hindrance induced by the CAAC ligand. In addition, the $^{carbene}C$–B bond in **4** [1.545(5) Å] is shorter than the comparable $^{carbene}C$–B bond in **2** [1.609(3) Å] and **3** [1.601(4) Å], but almost equal to reported CAAC-stabilized boron-centered monoradicals.[24] This can be explained by the strong σ-donor and better π-accepting abilities of the cyclic(alkyl)(amino) carbenes (CAACs) compared to classical *N*-heterocyclic carbenes (NHCs). The central benzene ring is aromatic, as shown from the uniform bond lengths, C15−C16: 1.391(4), C16−C17: 1.397(4), C15−C17: 1.401(4) Å which supports the emergence of the biradical character.

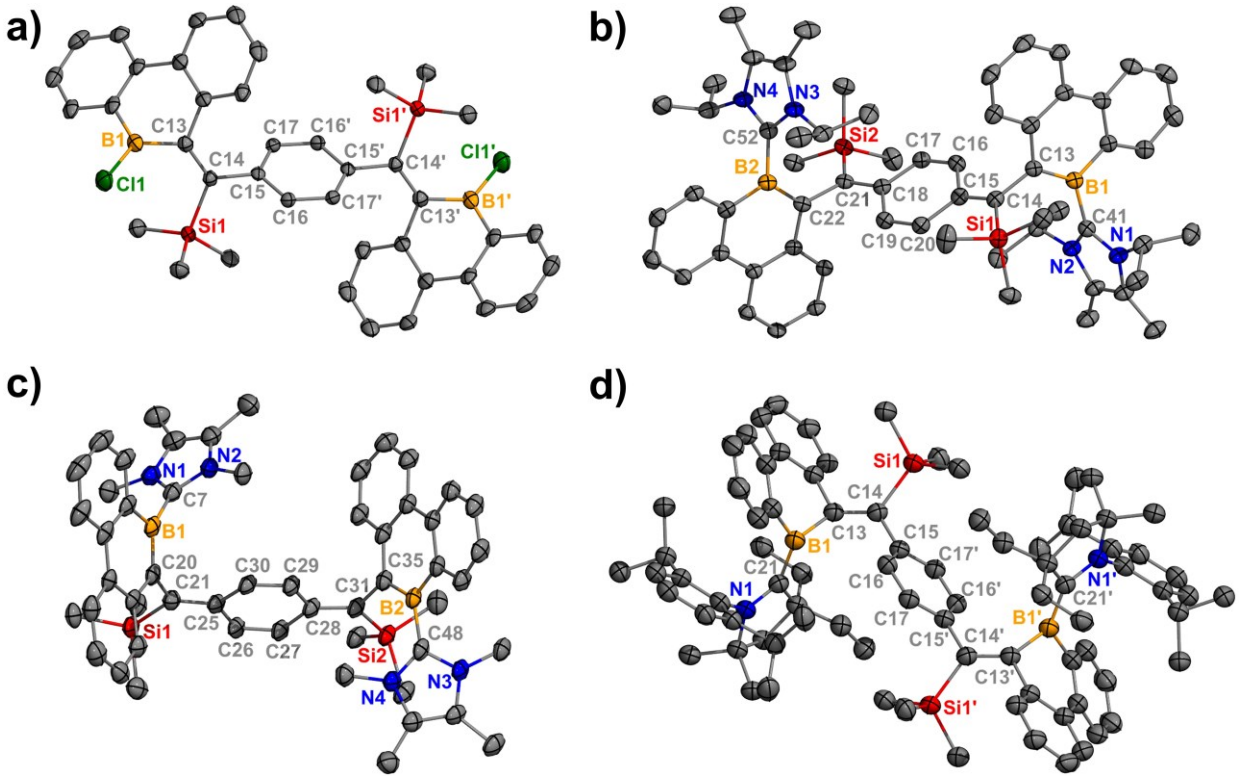

Figure 2. Molecular structures of **1** (a), **2** (b), **3** (c) and **4** (d). The anisotropic displacement parameters are depicted at the 50% probability level. Crystal data were collected at 100 K. Hydrogen atoms, and solvent molecules are omitted for clarity. Note: Compound **2** has two crystallographically identical molecules in the unit cell with similar bond lengths and angles. Only one is depicted for comparison purposes. Selected bond lengths (Å) and angles (°): **1**: B1−Cl1 1.764(3), B1−C13 1.545(4), C13−Cl14 1.366(4), ∠C13−C14−C15 121.6(2); **2**: B1−C13 1.469(4), B2−C22 1.473(3), C18−C21 1.372(3), C21−C22 1.500(3), C15−C14 1.373(3), C14−C13 1.494(3), C15−C16 1.456(3), C16−C17 1.353(3), C17−C18 1.451(3), C18−C19 1.458(3), C19−C20 1.351(3), C20−C15 1.459(3), B1−C41 1.604(3), B2−C52 1.609(3), ∠ C13−C14−C15 120.3(2), **3**: B1−C20 1.467(4), B2−C35 1.475(4), C20−C21 1.496(4), C21−C25 1.376(4), C25−C26 1.448(4), C26−C27 1.347(4), C27−C28 1.454(4), C28−C29 1.458(4), C29−C30 1.350(4), C30−C25 1.453(3), C28−C31 1.382(4), C31−C35 1.505(4), B1−C7 1.604(3), B2−C48 1.594(4), ∠C20−C21−C25 121.3(2); **4**: B1−C21 1.545(5), B1−C13 1.619(4), C15−C16 1.391(4), C16−C17 1.397(4), C15−C17 1.401(4), ∠C13−C14−C15 121.1(2).

The paramagnetic nature of **4** was confirmed by solution and solid-state EPR spectroscopy (Figure 3). In THF, the EPR spectrum of **4** displays a single broad signal centered at g = 2.004, with no observable hyperfine splitting, in agreement with EPR spectra observed for carbon-based PAH biradical systems.[18,19,22] The powder EPR spectrum of **4** displays low and high field transitions (ΔM_s = ±1) characteristic of organic spin triplets (S = 1); coinciding with a central transition determined through simulation to be a monoradical (S = ½) impurity originating from a single N– ^{carbene}C–B spin system.[17, 24c] The assignment of this impurity is consistent with our previously reported CAAC-stabilized borepin and borafluorene radicals, where the spin system is localized to the N–^{carbene}C–B moiety.[17,24] The point-dipole approximation employing the simulated zero-field splitting parameter $|D'|$ (2.62 mT) determined an average inter-spin distance of 10.2 Å, consistent with crystallographic measurements indicating a distance of approximately 9.57 Å between the centroids of the two N–^{carbene}C–B fragments. The half-field transition could not be clearly observed at room temperature due to its intensity being proportional to the r^{-6} inter-spin distance. However, the signal corresponding to the ΔMs = ±1 transitions were observable at 80 K and showed temperature dependence between 20-80 K; its intensity diminished as the temperature decreased, indicative of a singlet ground state with a thermally accessible triplet (Figure S35, right).

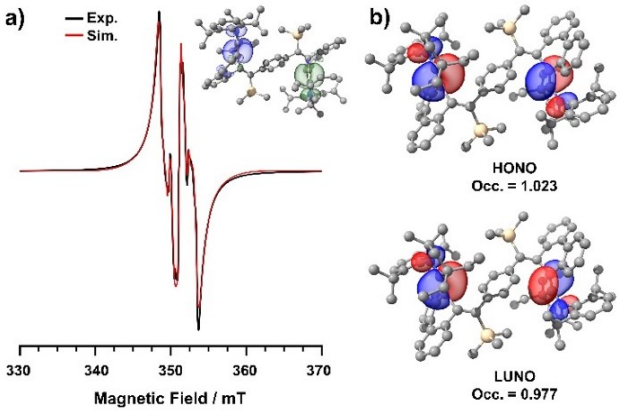

Figure 3. (a) Experimental and simulated powder X-band EPR spectrum of **4** at room temperature (simulation parameters: S = 1, g = [2.008 2.001 2.005], $|D'|$ = 2.62 mT, $|E'|$ = 0.10 mT ; S = ½, g_{iso} = 2.005, a(N) = 16 MHz, a(B) = 12 MHz; $w(S = ½)$ = 0.132; RMSD = 0.025) [Inset: Spin-density distribution of OSS **4** calculated at the BS-B3LYP-D3(BJ)/def2-TZVP (CPCM, THF) level of theory (isosurface = ± 0.003 e a_0^{-3}, green and blue correspond to regions α- and β-spin, respectively]. (b) Optimized CASSCF(2,2)/def2-TZVP natural orbitals and natural orbital occupancies for **4**.

The electronic structure and spin preferences of compound **4** were evaluated through theoretical calculations. Exploratory DFT studies were conducted at the B3LYP-D3(BJ)/def2-TZVP level of theory to assess the relative adiabatic energies of the closed-shell singlet (CSS), open-shell singlet (OSS) and triplet (T) electronic configurations. These calculations identified the OSS as the ground-state, while the triplet and CSS states were found to be +0.16 and +97.07 kJ mol^{-1} higher in energy, respectively. Furthermore, to investigate the magnetic exchange interaction of the OSS electronic configuration, broken symmetry DFT (BS-DFT) calculations were conducted. The analysis of the broken-symmetry wavefunction indicated a weak antiferromagnetic exchange interaction (H = -2J$S_A S_B$; J = -13 cm^{-1}) between the two paramagnetic centers. Additionally, the overlap integral ($|S^{\alpha\beta}|^2$) of the magnetically coupled orbitals approached zero (0.038) suggesting that the single occupied molecular orbitals (SOMOs) are non-coextensive.[25] This is a feature typically observed in disjointed paramagnetic species with significant biradical character.[26] The spin-density distribution plot derived from the BS-DFT wavefunction of compound **4** provides additional evidence for the presence of two localized paramagnetic centers. This plot reveals a localized region of α-spin density on one boraphenanthrene moiety and a distinct β-spin density on the other boraphenanthrene moiety (Figure 3a, inset). Moreover, calculated atomic spin populations indicate a nearly balanced distribution among nitrogen (± 24%), ^{carbene}carbon (± 32%), and boron (± 33%), atoms within the N–^{carbene}C–B units. (Table S4). Such values are consistent with spin populations previously calculated for related CAAC-stabilized boron radicals, in which the spin is found to be delocalized across the N–^{carbene}C–B moiety.[16,24]

For a more precise determination of the OSS-T energy gap ($\Delta E_{OSS\text{-}T}$) and to quantify the biradical character of compound **4** multideterminant *ab initio* calculations were employed. Complete active space self-consistent field (CASSCF) calculations were employed, using an active space of two electrons in two orbitals (CASSCF(2,2)/def2-TZVP) (refer to SI for investigations of an extended active space). An OSS-T energy gap of -0.14 kJ mol^{-1} was obtained upon the inclusion of dynamic electron correlation using the DLPNO-NEVPT2 method.[27a] For the CASSCF ground-state, the natural orbital occupation numbers (NOON) were determined to be 1.02 and 0.98, confirming an OSS electronic configuration for compound **4** (Figure 3b). Using these values, the biradical character (γ) of **4** was determined to be 0.95.[27b] The biradical character evident in compound **4** is markedly greater than that observed in recently reported boron PAH biradicals, which exhibit γ values ranging from 0.31 to 0.85 and are accompanied by larger OSS-Triplet gaps (0.21-6.28 kJ mol^{-1}).[16,17,20]

The photophysical properties of compounds **2** and **3** were investigated in detail using standard optical spectroscopic techniques (Table 1). The absorption spectra of compounds **2** and **3** in THF show two major bands at ca. 381 and 520 nm, with shoulder peaks at 364 and 420 nm, respectively (Figure 4). The high energy absorption peaks of **2** and **3** (381 and 363 nm) are red-shifted by approximately 114-130 nm compared to phenanthrene, which has a strong absorption band at 250 nm with a shoulder peak at 295 nm and a weak broad vibronic absorption band from 290-350 nm.[28] Time-dependent density functional theory (TD-DFT) calculations (CAM-B3LYP-D3(BJ)/def2-TZVP, (CPCM, THF)) conducted on **2** and **3** showed that the lowest energy bands centered at 520 nm consists of two charge-transfer (CT) transitions ($S_1 \leftarrow S_0$ and $S_2 \leftarrow S_0$) from the 9-boraphenanthrene units to *p*-quinodimethane (Table S3). The low intensity of these bands can be attributed to the near perpendicular orientation of the boraphenanthrene and *p*-quinodimethane planes in the ground state for both **2** and **3**. This arrangement hinders the orbital overlap between their respective π orbitals, resulting in symmetry-forbidden transitions that are weakly allowed. The shoulder band (S_3) at 420 nm involves π→π* local excitations centered on the boraphenanthrene fragments, while the intense band at 380 nm features similar π→π* local excitations centered on the *p*-quinodimethane fragment. Conversion of **1** into diradical **4** leads to a bathochromic shift in absorbance. Compound **4** exhibits low energy absorption features at 520 and 472 nm which resemble the low-lying singlet excited states typical for singlet biradicaloids and are suggested to originate from a doubly excited electronic configuration.[18]

Table 1. Photophysical properties of 2 and 3.

Parameters	Compound **2**	Compound **3**
λ_{abs} (nm)	381, 520	364, 520
ε (10^5 M^{-1}cm^{-1})	2.5, 0.13	1.1, 0.23
$\lambda_{em,\ liq}$(nm)	441, 643	441, 643
$\lambda_{em,sol}$(nm)	631	683
Φ_{liq} (%)	6.3	3.3
Φ_{sol} (%)	3.5	1.2
Lifetime(ns) ($\tau_{440nm,\ THF}$)	15	11.33 (89%) 4.14 (11%)
Lifetime(ns) ($\tau_{640nm,\ THF}$)	3.73	0.55 (83%) 3.25 (17%)
Lifetime(ns) (τ_{solid})	3.78	5.18

aValues in parentheses indicate the relative amplitude weightings of the pre-exponential factors. Lifetimes measured at λ_{exct} = 340 nm.

Despite the synthetic advances in the organoboron field, most of the reported boron-doped PAHs show a single photoluminescence feature in the blue to green region of the visible spectrum owing to their larger HOMO–LUMO energy gap and poor orbital overlap between donor-acceptor moieties.[1-11] Conversely, the literature on dual emissive or near-IR (NIR) emissive boron-embedded PAHs are comparatively limited.[26-27,29-30] Dual emission phenomena generally arise from two geometrically distinct singlet excited states, each possessing unique emission characteristics.[31] Achieving dual emission with NIR properties remains a significant challenge, owing to the absence of well-defined design principles and the tendency for these molecules to undergo vibrational relaxation in the excited states, resulting in single-color emission from the lowest energy excited state to the ground state.[31-32] However, when excited at 380 nm, compounds **2** and **3** exhibit dual emission peaks in THF at 441 and 643 nm (Figure 5), with a total quantum efficiency (Φ) of 6.3 and 3.3%, respectively. The higher energy band at 441 nm displays a structured pattern, suggesting a locally-excited (LE) emission, while the broad 643 nm low energy emission feature may be associated with increased conjugation in the excited state due to rotation of the boraphenanthrene moieties. This dual emission mechanism, known as excited state conjugation enhancement (ESCE) describes the red-shifted emission observed in a conjugated system upon excitation, resulting from increased conjugation length.[33-34]

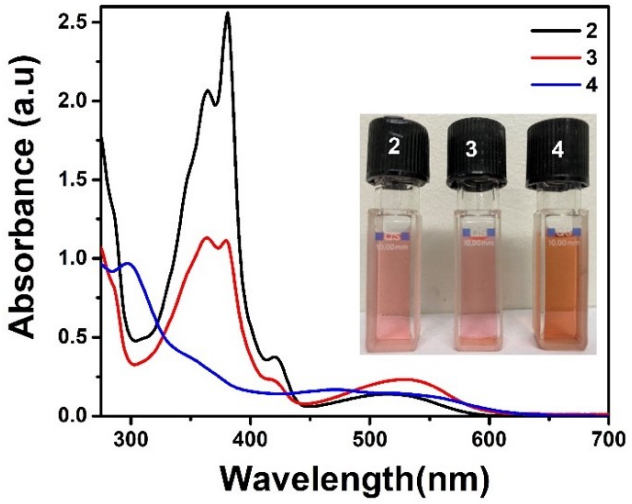

Figure 4. UV-Vis absorption spectra of **2** (black), **3** (red) and **4** (blue) in THF (1×10^{-5} M) at ambient conditions.

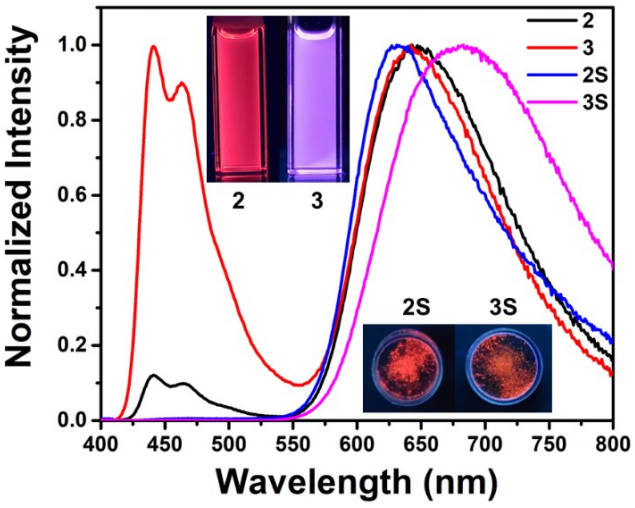

Figure 5. Normalized photoluminescnece spectra of **2** (black, λ_{exct} = 350 nm) and **3** (red, λ_{exct} = 350 nm) in THF (1×10–5 M) at ambient conditions and **2** (2S, blue, λexct = 350 nm) and **3** (3S, pink, λ_{exct} = 350 nm) in the solid-state.

To explore the dual emission process in **2** and **3**, a comprehensive examination of the S_1 potential energy surface (PES) was conducted using TD-DFT. A relaxed PES scan of **3** initiated from the Franck-Condon (FC) state, located two distinct minima (Figure 6a): a LE state, resembling the ground state minimum, and an ESCE state, characterized by a rotation of both boraphenanthrene fragments (± 49°) toward the *p*-quinodimethane plane. The geometry of the LE state exhibits partial rotation of a single boraphenanthrene unit, -20° relative to the FC state geometry. The ESCE state is energetically more favorable, situated -36 kJ mol^{-1} below the LE state. The calculated vertical emission energies correspond well with the experimental data, with the LE and ESCE states exhibiting vertical emission energies of 476 and 698 nm, respectively. Examination of the HOMO and HOMO-1 orbitals in the ESCE state reveals π orbital mixing between the boraphenanthrene and *p*-quinodimethane units, which is only observed in the locally excited (LE) state and absent in the ground state (S_0) (Figure 6a and 6b). As a result, the emission from the LE state can be assigned to a localized emission centered on the boraphenanthrene units, while the lower-energy ESCE emission stems from the rotation and subsequent enhanced conjugation between boraphenanthrene and *p*-quinodimethane moieties.

Furthermore, the origin of the dual emission is also supported by the time-resolved decay measurements (Table 1). Compound **2** fits a mono-exponential decay monitored at 440 and 643 nm, with PL lifetimes of τ = 15 ns (100%) and τ = 3.73 ns (100%), respectively (Figure S17). Meanwhile, the time-resolved decay curve for **3** displays two components with PL lifetimes of 4.14 ns (11%) and 11.33 ns (89%) at 440 nm, and 0.55 ns (83%) and 3.25 ns (17%) at 643 nm, respectively (Figures S29 and S30). From PL lifetime analysis, shorter lifetimes are assigned to the ESCE emission, and longer lifetimes are assigned to LE emission. Both compounds are red emissive in the solid-state. Solid samples **2** and **3** display a single emission peak at 631 and 683 nm and a broad emission tail up to 850 nm (Figure 5). Interestingly, in the solid-state, an unusual 12 nm hyposochromic shift is observed for **2** while the emission of **3** is shifted into the red region by 50 nm with respect to their liquid-state fluorescence emission in THF solvent ($\lambda_{max,\ solid}$ = 443 nm). This can be explained by analyzing the molecular structures. Based on the crystal data, the 9-boraphenanthrene unit of **2** is almost perpendicular to its *p*-quinodimethane moiety. The dihedral angle between the 9-boraphenanthrene and *p*-quinodimethane unit is 84.9° for **2** and 75.3° for **3**. As a result, the ESCE process in the solid-state is not as prominent as in the solution state for **2**. Also, the presence of isopropyl groups on the ^{i}Pr-NHC in **2** prevents and restricts the extended ESCE process in the solid-state.

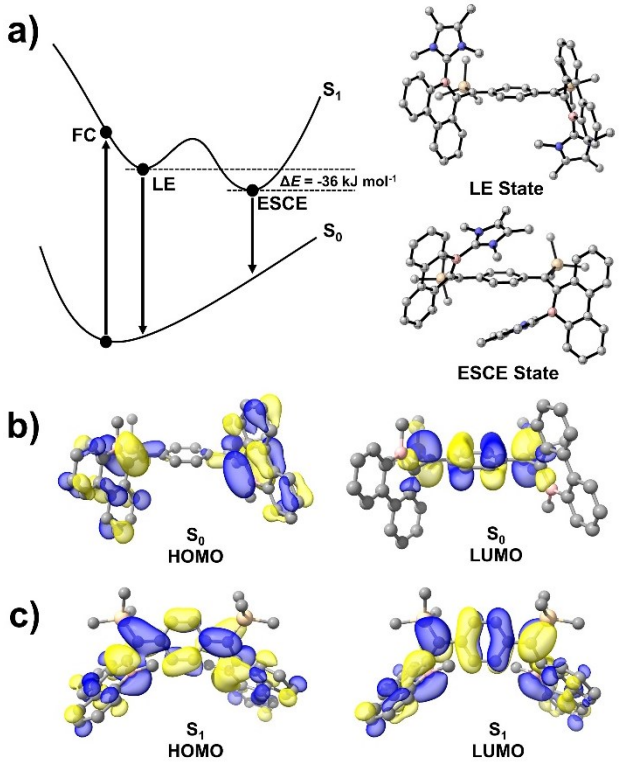

Figure 6. (a) Potential energy surface depicting the ESCE dual emission process for **3**, and optimized LE and ESCE geometries. (b) Ground (S_0) and (c) ESCE state (S_1) frontier molecular orbitals of **3**, calculated at the CAM-B3LYP-D3(BJ)/def2-TZVP//B3LYP-D3(BJ)/def2-TZVP (CPCM, THF) level of theory (hydrogen atoms and IMe_4 ligands omitted for clarity).

In contrast, the red-shifted solid-state emission for **3** is produced via an extended ESCE process in the solid-state due to less steric

hindrance. The small NHCs and reduced dihedral angle between 9-boraphenanthrene and the *p*-quinodimethane unit play a significant role to yield a bathochromic shift for **3** in comparison to the solution state emission. Both compounds show a mono-exponential decay at 631 and 683 nm with lifetimes τ = 3.78 ns (100%) and 5.18 ns (100%), respectively (Figures S22 and S34). Furthermore, the solid-state quantum yields are 3.5% and 1.2%, respectively. The lower quantum yield in the solid-state of **2** and **3** can be explained by the fluorescence quenching related to the small energy gap and fast radiative decay process. Additionally, the 1931 Commission Internationale de l'éclairage (CIE) chromaticity coordinates are calculated from the corresponding photoluminescence spectra. The CIE coordinates for **2** and **3** in THF are found to be (0.56, 0.30) and (0.30, 0.18) which is in the red and violet-white region, respectively (Figures S16 and S25). The solid samples of **2** and **3** showed red light emission with CIE coordinates of (0.65, 0.34) and (0.66, 0.33) respectively (Figures S20 and S32).

■ CONCLUSIONS

In conclusion, we report the first example of neutral bis(9-boraphenanthrene) and its stable biradical, which are obtained by the reduction of chloroboracycle (**1**) with KC_8 in presence of NHCs and CAAC, respectively. The NHC-stabilized bis(9-boraphenanthrene)s (**2**-**3**) show intramolecular charge transfer absorption from the 9-boraphenanthrene units to *p*-quinodimethane, exhibiting intriguing dual (red-shifted) emission in solution due to excited state conjugation enhancement (ESCE). The open-shell singlet biradical form of bis(9-boraphenanthrene) is isolated using the CAAC ligand, where experimental and theoretical results identify **4** to be a disjointed biradical species, exhibiting the highest reported degree of biradical character among all boron-based PAHs currently known. This work capitalizes on new ring expansion methodology to obtain six-membered boraphenanthrene heterocycles, which hold great potential to produce a range of boron heterocycles with intriguing optical and/or magnetic properties that would otherwise be inaccessible.

■ ASSOCIATED CONTENT

Supporting Information

The supporting information file contains experimental details, NMR spectra, photophysical data, single-crystal X-ray diffraction data, and computational details (PDF). Crystallographic data for **1**, **2**, **3**, and **4**, (CIF) has been submitted to CCDC (2271409-2271412). The CIF can be obtained free of charge from the Cambridge Crystallographic Data center via www.ccdc.cam.ac.uk/structures.

■ AUTHOR INFORMATION

Corresponding Authors

David J. D. Wilson – Department of Biochemistry and Chemistry, La Trobe Institute for Molecular Science, La Trobe University, Melbourne 3086 Victoria, Australia; orcid.org/0000-0002-0007-4486
Email: david.wilson@latrobe.edu.au
Robert J. Gilliard Jr – Department of Chemistry, Massachusetts Institute of Technology, Massachusetts 02139, United States; orcid.org/0000-0002-8830-1064
Email: gilliard@mit.edu

Author Contributions

Samir Kumar Sarkar– Department of Chemistry, Massachusetts Institute of Technology, Massachusetts 02139, United States; orcid.org/0000-0003-3822-6083
Kimberly K. Hollister – Department of Chemistry, Massachusetts Institute of Technology, Massachusetts 02139, United States; orcid.org/0000-0001-9024-4436
Andrew Molino – Department of Biochemistry and Chemistry, La Trobe Institute for Molecular Science, La Trobe University, Melbourne 3086 Victoria, Australia; orcid.org/0000-0002-0954-9054
Akachukwu D. Obi – Department of Chemistry, University of Virginia, Charlottesville, Virginia 22904, United States; orcid.org/0000-0001-7118-7931
Chun-Lin Deng – Department of Chemistry, Massachusetts Institute of Technology, Massachusetts 02139, United States; orcid.org/0000-0003-0236-736X
Bi Youan E. Tra – Department of Chemistry, Massachusetts Institute of Technology, Massachusetts 02139, United States; orcid.org/ 0000-0003-1700-4369
Brennan M. Stewart – Department of Chemistry, University of Virginia, Charlottesville, Virginia 22904, United States; orcid.org/ 0000-0002-6039-2929
Diane A. Dickie – Department of Chemistry, University of Virginia, Charlottesville, Virginia 22904, United States; orcid.org/ 0000-0003-0939-3309

Notes

The authors declare no competing financial interests.

■ ACKNOWLEDGMENT

We are grateful to the Arnold & Mabel Beckman Foundation for a Beckman Young Investigator award. We also thank the Alfred P. Sloan Foundation for a Sloan Research Fellowship. Generous allocation of computing resources from the National Computational Infrastructure (NCI), Intersect, and La Trobe University are acknowledged.

■ REFERENCES

(1) (a) Fittig, R.; Ostermayer, E. Ueber das Phenanthren, einen neuen Kohlenwasserstoff im Steinkohlentheer. *Justus Liebigs Ann. Chem.* **1873**, *166*, 361–382. (b) Floyd, A. J.; Dyke, S. F.; Ward, S. E. The Synthesis of Phenanthrenes. *Chem. Rev.* **1976**, *76*, 509–562. (c) Boden, B. N.; Jardine, K. J.; Leung, A. C. W.; MacLachlan, M. J. Tetraalkoxyphenanthrene: A New Precursor for Luminescent Conjugated Polymers. *Org. Lett.* **2006**, *8*, 1855–1858.

(2) Li, J.-Y.; Chang, H.-I.; Feng, C.-N.; Wu, Y.-T. Rotation of Aryl Groups in 9,10-Diarylphenanthrenes: Does the Rotational Barrier Become Lower as the Backbone Becomes More Crowded?. *Org. Lett.* **2016**, *18*, 6444–6447.

(3) (a) Kaleta, J.; Mazal, C. A Triangular Macrocycle Altering Planar and Bulky Sections in Its Molecular Backbone. *Org. Lett.* **2011**, *13*, 1326–1329. (b) Guo, S.; Jin, X.; Zhang, D.; Zhou, H.; Wang, G.; Miao, Y.; Huang, J.; Zhang, Z.; Wang, H.; Su, J. Phenanthrene-based deep-blue fluorophores with balanced carrier transport ability for high-performance OLEDs with a CIEy < 0.04. *J. Mater. Chem. C* **2022**, *10*, 14711–14721. (c) Toya, M.; Omine, T.; Ishiwari, F.; Saeki, A.; Ito, H.; Itami, K. Expanded [2,1][n]Carbohelicenes with 15- and 17-Benzene Rings. *J. Am. Chem. Soc.* **2023**, *145*, 11553–11565. (d) Green, P. B.; Lecina, O. S.; Albertini, P. P.; Loiudice, A.; Buonsanti, R. Colloidal-ALD-Grown Metal Oxide Shells Enable the Synthesis of Photoactive Ligand/Nanocrystal Composite Materials. *J. Am. Chem. Soc.* **2023**, *145*, 8189–8197.

(4) Escande, A.; Ingleson, M. J. Fused Polycyclic Aromatics Incorporating Boron in the Core: Fundamentals and Applications. *Chem. Commun.* **2015**, *51*, 6257– 6274.

(5) Wakamiya, A.; Yamaguchi, S. Designs of Functional π-Electron Materials based on the Characteristic Features of Boron. *Bull. Chem. Soc. Jpn.* **2015**, *88*, 1357–1377.

(6) Hirai, M.; Tanaka, N.; Sakai, M.; Yamaguchi, S. Structurally constrained boron-, nitrogen-, silicon-, and phosphorus-centered polycyclic π-conjugated systems. *Chem. Rev.* 2019, *119*, 8291– 8331.

(7) Farrell, J. M.; Mützel, C.; Bialas, D.; Rudolf, M.; Menekse, K.; Krause, A.-M.; Stolte, M.; Würthner, F. Tunable Low-LUMO Boron-Doped Polycyclic Aromatic Hydrocarbons by General One-Pot C–H Borylations. *J. Am. Chem. Soc.* **2019**, *141*, 9096–9104.

(8) Yang, M.; Park, I. S.; Yasuda, T. Full-Color, Narrowband, and High-Efficiency Electroluminescence from Boron and Carbazole Embedded Polycyclic Heteroaromatics. *J. Am. Chem. Soc.* **2020**, *142*, 19468–19472.

(9) Choi, H.; Ogi, S.; Ando, N.; Yamaguchi, S. Dual Trapping of a Metastable Planarized Triarylborane π-System Based on Folding and Lewis Acid–Base Complexation for Seeded Polymerization. *J. Am. Chem. Soc.* **2021**, *143*, 2953–2961.

(10) (a) Caruso, A., Jr.; Siegler, M. A.; Tovar, J. D. Synthesis of Functionalizable Boron-Containing π-Electron Materials that Incorporate Formally Aromatic Fused Borepin Rings. *Angew. Chem., Int. Ed.* **2010**, *49*, 4213–4217. (b) Levine, D. R.; Siegler, M. A.; Tovar, J. D. Thiophene-fused borepins as directly functionalizable boron-containing pi-electron systems. *J. Am. Chem. Soc.* **2014**, *136*, 7132–7139.

(11) Bartholome, T. A.; Kaur, A.; Wilson, D. J. D.; Dutton, J. L.; Martin, C. D. The 9-Borataphenanthrene Anion. *Angew. Chem., Int. Ed.* **2020**, *59*, 11470–11476.

(12) Yang, W.; Krantz, K. E.; Dickie, D. A.; Molino, A.; Wilson, D. J. D.; Gilliard, R. J., Jr. Crystalline BP-Doped Phenanthryne via Photolysis of The Elusive Boraphosphaketene. *Angew. Chem., Int. Ed.* **2020**, *59*, 3971–3975.

(13) Caruso, A., Jr.; Siegler, M. A.; Tovar, J. D. Synthesis of Functionalizable Boron Containing π-Electron Materials that Incorporate Formally Aromatic Fused Borepin Rings. *Angew. Chem., Int. Ed*. **2010**, *49*, 4213−4217.

(14) Schickedanz, K.; Trageser, T.; Bolte, M.; Lerner, H.-W.; Wagner, M. A boron-doped helicene as a highly soluble, benchtop-stable green emitter. *Chem. Commun.* **2015**, *51*, 15808–15810.

(15) Hertz, V. M.; Bolte, M.; Lerner, H.-W.; Wagner, M. Boron-Containing Polycyclic Aromatic Hydrocarbons: Facile Synthesis of Stable, Redox-Active Luminophores. *Angew. Chem., Int. Ed.* **2015**, *54*, 8800–8804.

(16) (a) Gärtner, A; Meier, L; Arrowsmith, M; Dietz, M; Krummenacher, I; Bertermann, R; Fantuzzi, F; Braunschweig, H. Highly Strained Arene-Fused 1,2-Diborete Biradicaloid. *J. Am. Chem. Soc.* **2022**, *144*, 46, 21363–21370. (b) Gärtner, A.; Meier, L.; Arrowsmith, M.; Dietz, M.; Krummenacher, I.; Bertermann, R.; Fantuzzi, F.; Braunschweig, H. A. Highly Strained Arene-Fused 1,2-Diborete Biradicaloid. *J. Am. Chem. Soc.* **2022**, *144*, 21363–21370. (c) Dietz, M; Arrowsmith, M; Drepper, K; Gärtner, A; Krummenacher, I; Bertermann, R; Finze, M; Braunschweig, H. Structure and Electronics of a Series of CAAC-Stabilized Diboron-Doped Acenes from 1,4-Diboranaphthalene to 6,13-Diborapentacene. *J. Am. Chem. Soc.* **2023**, *145,* 15001–15015.

(17) Saalfrank, C.; Fantuzzi, F.; Kupfer, T.; Ritschel, B.; Hammond, K.; Krummenacher, I.; Bertermann, R.; Wirthensohn, R.; Finze, M.; Schmid, P.; Engel, V.; Engels, B.; Braunschweig, H. CAAC-Stabilized 9,10-Diboraanthracenes─Acenes with Open-Shell Singlet Biradical Ground States. *Angew. Chem., Int. Ed.* **2020**, *59*, 19338–19343.

(18) (a) Sun, Z.; Lee, S.; Park, K. H.; Zhu, X.; Zhang, W.; Zheng, B.; Hu, P.; Zeng, Z.; Das, S.; Li, Y.; Chi, C.; Li, R.-W.; Huang, K.-W.; Ding, J.; Kim, D.; Wu, J. Dibenzoheptazethrene Isomers with Different Biradical Characters: An Exercise of Clar's Aromatic Sextet Rule in Singlet Biradicaloids. *J. Am. Chem. Soc.* **2013**, *135*, 18229–18236. (b) Kuriakose, F; Commodore, M; Hu, C; Fabiano, C. J; Sen, D; Li, R. R; Bisht, S; Üngör, Ö; Lin, X; Strouse, G. F; DePrince, A. E. III; Lazenby, R. A; Mentink-Vigier, F; Shatruk, M; Alabugin, I. V. Design and Synthesis of Kekulè and Non-Kekulè Diradicaloids via the Radical Periannulation Strategy: The Power of Seven Clar's Sextets. *J. Am. Chem. Soc*. **2022**, *144*, 23448–23464. (c) Xu, X; Takebayashi, S; Hanayama, H; Vasylevskyi, S; Onishi, T; Ohto, T; Tada, H; Narita, A. 6,6′ -Biindeno[1,2-b]anthracene: An Open-Shell Biaryl with High Diradical Character. *J. Am. Chem. Soc*. **2023**, *145*, 3891–3896.

(19) Zhe Sun, Zebing Zeng, and Jishan Wu. Zethrenes, Extended p-Quinodimethanes, and Periacenes with a Singlet Biradical Ground State. *Accounts of Chemical Research* **2014**, *47* (8), 2582–2591.

(20) Guo, J.; Dou, C.; Wang, Y. Boron-Containing Organic Diradicaloids: Dynamically Modulating Singlet Diradical Character by Lewis Acid-Base Coordination. *J. Am. Chem. Soc.* **2021**, *143*, 18272–18279.

(21) Clar, E. The Aromatic Sextet; Wiley: London, 1972.

(22) Solà, M. Forty Years of Clar's Aromatic π-Sextet Rule. *Front. Chem.* **2013**, *1*, 22, DOI: 10.3389/fchem.2013.00022.

(23) (a) Podall, H.; Foster, W. E.; Giraitis, A. P. Catalytic Graphite Inclusion Compounds. I. Potassium Graphite as a Polymerization Catalyst. *J. Org. Chem.* **1958**, 23, 82–85. (b) Kratz, T; Kuhn, N. Synthesis of Imidazol-2-ylidenes by Reduction of Imidazole-2(3H)-thiones. *Synthesis* **1993**, *6*, 561–562. (c) Lavallo, V.; Canac, Y.; Prasang, C.; Donnadieu, B.; Bertrand, G. Stable Cyclic (Alkyl)(Amino)Carbenes as Rigid or Flexible, Bulky, Electron-Rich Ligands for Transition-Metal Catalysts: A Quaternary Carbon Atom Makes the Difference. *Angew. Chem., Int. Ed.* **2005**, *44*, 5705–5709. (d) Braunschweig, H.; Kupfer, T. Recent developments in the chemistry of antiaromatic boroles. *Chem. Commun.* **2011**, *47*, 10903–10914.

(24) (a) Hollister, K. K.; Yang, W.; Mondol, R.; Wentz, K. E.; Molino, A.; Kaur, A.; Dickie, D. A.; Frenking, G.; Pan, S.; Wilson, D. J. D.; Gilliard, R. J. Isolation of Stable Borepin Radicals and Anions. *Angew. Chem., Int. Ed.* **2022**, *61*, e2022025. (b) Yang, W.; Krantz, K. E.; Freeman, L. A.; Dickie, D. A.; Molino, A.; Frenking, G.; Pan, S.; Wilson, D. J. D.; Gilliard, R. J., Jr. Persistent Borafluorene Radicals. *Angew. Chem., Int. Ed.* **2020**, *59*, 3850–3854.

(25) (a) Soda, T.; Kitagawa, Y.; Onishi, T.; Takano, Y.; Shigeta, Y.; Nagao, H.; Yoshioka, Y.; Yamaguchi, K. Ab Initio computations of effective exchange integrals for H–H, H–He–H and Mn_2O_2 complex: Comparison of broken-symmetry approaches. *Chem. Phys. Lett.* **2000**, *319*, 223–230. (b) Neese, F. Definition of Corresponding Orbitals and the Diradical Character in Broken Symmetry DFT Calculations on Spin Coupled Systems. *J. Phys. Chem. Solids* **2004**, *65*, 781–785.

(26) Dougherty, D. A. Spin Control in Organic Molecules. *Acc. Chem. Res.* **1991**, *24* (3), 88–94.

(27) (a) Guo, Y.; Sivalingam, K.; Valeev, E. F.; Neese, F. SparseMaps─A systematic infrastructure for reduced-scaling electronic structure methods. III. Linear-scaling multireference domain-based pair natural orbital N-electron valence perturbation theory. *J. Chem. Phys.* **2016**, *144*, 094111. (b) Yamanaka, S; Okumura, M; Nakano, M; Yamaguchi, K. EHF theory of chemical reactions Part 4. UNO CASSCF, UNO CASPT2 and R(U)HF coupled-cluster (CC) wavefunctions, *J. Mol. Struct.: THEOCHEM*, **1994**, *310*, 205–218.

(28) Pavlopoulos, T. G.; Search for vibronic spin–orbit interactions in the triplet-manifold of phenanthrene N-heterocyclic analogues. *Journal of Photochemistry and Photobiology A: Chemistry*. **2002**, *149*, 45–54.

(29) Farrell, J. M.; Mützel, C.; Bialas, D.; Rudolf, M.; Menekse, K.; Krause, A.-M.; Stolte, M.; Würthner, F. Tunable Low-LUMO Boron-Doped Polycyclic Aromatic Hydrocarbons by General One-Pot C-H Borylations. *J. Am. Chem. Soc.* **2019**, *141*, 9096–9104.

(30) Osumi, S.; Saito, S.; Dou, C.; Matsuo, K.; Kume, K.; Yoshikawa, H.; Awaga, K.; Yamaguchi, S. Boron-Doped Nanographene: Lewis Acidity, Redox Properties, and Battery Electrode Performance. *Chem. Sci.* **2016**, *7*, 219–227.

(31) Lakowicz, J. R. *Principles of fluorescence spectroscopy*, Springer, New York, NY, 3rd edn, 2006.

(32) Kasha, M. Characterization of Electronic Transitions in Complex Molecules. *Discuss. Faraday Soc.*, **1950**, 9, 14–19.

(33) Behera, S. K.; Park, S. Y.; Gierschner, J. Dual Emission: Classes, Mechanisms, and Conditions. *Angew. Chem., Int. Ed*. **2021**, *60*, 22624–22638.

(34) Gierschner, J.; Shi, J.; Milián-Medina, B.; Roca-Sanjuán, D.; Varghese, S.; Park, S. Luminescence in Crystalline Organic Materials: From Molecules to Molecular Solids. *Adv. Opt. Mater.* **2021**, 9, 2002251.

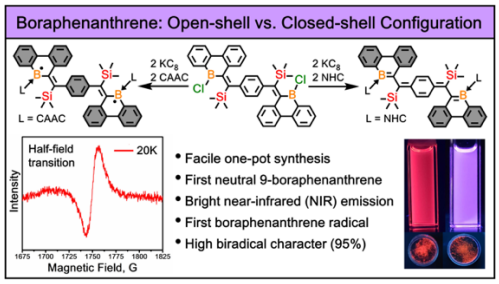

Insert Table of Contents artwork here